INSTITUTE OF PHYSICS PUBLISHING JOURNAL OF PHYSICS: CONDENSED MATTER

J. Phys.: Condens. Matter **15** (2003) S1379–S1402 PII: S0953-8984(03)55821-0

Designing magnetic composite materials using aqueous magnetic fluids

José Alberto Galicia[1], Olivier Sandre[1], Fabrice Cousin[2], Dihya Guemghar[1], Christine Ménager[1] and Valérie Cabuil[1]

[1] Laboratoire Liquides Ioniques et Interfaces Chargées—Equipe Colloïdes Inorganiques, UMR 7612 CNRS/Université Pierre et Marie Curie (Paris 6), 4 place Jussieu, case 63—75252 Paris Cedex 05, France

[2] Laboratoire Léon Brillouin, UMR 12 CNRS/CEA CEA-Saclay—91191, Gif-sur-Yvette, France

Received 8 November 2002
Published 7 April 2003
Online at stacks.iop.org/JPhysCM/15/S1379

Abstract

In this paper, we report on how to take advantage of good knowledge of both the chemistry and the stability of an aqueous magnetic colloidal suspension to realize different magnetic composites. The osmotic pressure of the magnetic nanoparticles is set prior to the realization of the composite to a given value specially designed for the purpose for each hybrid material: magnetic particles in polymer networks, particles as probes for studying the structure of clay suspensions and shape modification of giant liposomes.

First, we show that the introduction of magnetic particles in polyacrylamide gels enhances their Young modulus and reduces the swelling caused by water. The particles cause both a mechanical and an osmotic effect. The latter is strongly dependent on the ionic strength and is attributed to an attraction between particles and the polymeric matrix.

In the second part, we determine the microscopic structure of suspensions of laponite as a function of concentration, by combining SANS and magneto-optical experiments with the probes. This study requires conditions suitable for including the magnetic particles as probes without disturbing the clay suspensions.

The third part presents giant magnetoliposomes, which encapsulate magnetic nanoparticles. Shape transitions are obtained with either a magnetic field or an osmotic stress.

Overview

Smart materials, meaning materials that respond to an external stimulus, can be obtained by associating magnetic nanoparticles with a polymeric or a lyotropic matrix. The resulting composite materials exhibit a response when they are subjected to a magnetic field of low intensity (typically less than 0.1 T) or to a magnetic field gradient. Different procedures can

be imagined for producing such materials: the magnetic particles can be either synthesized directly inside a host matrix, or synthesized first, then mixed with the other component of the composite. In recent years, magnetic nanoparticles have been successfully introduced in glass [1], polymeric gels [2, 3], lyotropic systems (nematics [4], smectics [5]), microscopic colloids (emulsions [6], latexes [7], liposomes [8]). They can be used as probes, in order to characterize the dynamics (and subsequently structure) of the medium through the analysis of their magneto-optical response [9], or they can be introduced as a magnetic load, in order to obtain field-dependent materials [5, 10, 11].

In efforts to improve the homogeneity of the resulting composite material, the colloidal stability of both components of the composite is of utmost importance. The colloidal dispersion of magnetic particles has thus to be stable in the chemical and physicochemical stability domains of the second system. The possibility of an eventual chemical incompatibility between the nanometric magnetic particles and the host colloid has to be examined first. A modification of the pH, an increase of the ionic strength and/or adsorption or desorption of the charge-determining species or of the surfactants can occur during the mixing process or a few weeks after, the latter case being especially harmful, because it can go unnoticed and lead to important interpretation errors. The chemistry of magnetic colloids is now sufficiently well developed that one can succeed in preventing such problems. As soon as the chemical stability of both colloidal systems is controlled, interactions in the binary system have to be monitored. In fact, each colloidal system is characterized by its own osmotic pressure Π. Thus it is roughly the case that the system that has the higher osmotic pressure will impose its own pressure on the other one which can then be destabilized [12]. The osmotic pressures of the two components should thus be of the same order of magnitude for the realization of the binary system.

The aim of this paper is to illustrate this comment by describing how it has been possible during recent years to design various magnetic composite systems always using the same well-defined magnetic material: an aqueous dispersion of citrate-coated maghemite nanoparticles, which will be denoted hereafter as CitMF [13]. Three examples are presented, resulting from the association of CitMF with several hosts, the latter being (i) a polymeric network, (ii) a gel of inorganic particles and (iii) a lyotropic system. In the first case, the polymer is a polyacrylamide cross-linked network. The intention was to trap the nanoparticles inside the mesh of the network and to compare the composite material with the undoped polymer. In the second case, the nanoparticles were introduced in aqueous dispersions of a clay (laponite) in order to test the structure of those inorganic gels and to test the hypothesis of microscopic liquid pockets coexisting with solid domains [14]. In the third case, CitMF was encapsulated inside liposomes, thus enabling us to cause them to elongate under a magnetic field or to generate migration of them under a field gradient. Among the three composite systems, laponite clay suspensions and magnetoliposomes have already been described extensively in former publications, whereas the results on the thermodynamics of ferrogels (swelling and elasticity) have not been published before and are therefore presented in more detail in this paper.

1. Properties of aqueous dispersions of citrate-coated particles (CitMF)

1.1. Getting CitMF

The maghemite nanoparticles are chemically synthesized in water by coprecipitation of $FeCl_2$ and $FeCl_3$ in an alkaline solution [15]. Due to the strong absorption of short-wavelength light by iron oxide, maghemite ferrofluids exhibit a characteristic orange colour. The colloidal particles have a quasi-spherical shape and their diameters after synthesis range between 3 and 15 nm

with a rather large polydispersity. Their size distribution is described by a log-normal law with a modal diameter d_0 around 7 nm ($\ln d_0 = \langle \ln d \rangle$) and a standard deviation $\sigma = 0.35$. When necessary, the polydispersity can be reduced by a size-sorting process to get suspensions with d_0 varying from 6 to 10 nm and $\sigma = 0.1$ [16]. In order to get stable suspensions from pH 4 to 10, particles are coated with citrate species. The adsorption equilibrium of citrate leads to an inevitable residual ionic strength $I = \frac{1}{2}\sum_i c_i z_i^2$; hence $I = 6[\mathrm{Cit}^{3-}]_{\mathrm{free}}$ due to the unadsorbed citrate species (Cit^{3-}) in equilibrium with the adsorbed ones and their Na^+ counterions. This equilibrium avoids decreasing the ionic strength under a given concentration that depends on the pH. At pH 7, the adsorption plateau is reached for a concentration of $[\mathrm{Na_3Cit}]$ in solution equal to 2×10^{-3} mol l^{-1} [17]. The particle's surface charge is negative, saturated at a value of 2 charges nm^{-2}. Above pH 10 citrate desorbs, while below pH 4 the surface charge density of these citrate-coated particles becomes insufficient to ensure electrostatic repulsion.

1.2. Phase behaviour of CitMF

The stability of CitMF has been the object of numerous studies in recent years [13, 18–21]. It exhibits a very rich behaviour due to two specific features: the presence of adsorbed citrate ligands and the magnetic dipolar interactions.

In such systems, the main interaction between particles is the electrostatic repulsion, which stabilizes the system over a wide range of salinity. In addition, the presence of citrate at the surface of the particles provides a steric repulsion at short range that ensures stability for high salinity [13] and prevents irreversible aggregation, which usually occurs in electrostatically stabilized colloidal systems. These two repulsive interactions ensure that all transitions are reversible whatever the experimental conditions. Magnetic dipolar interactions ensure that attractive interactions occur in the system on a larger range than van der Waals ones and allow tuning of the balance between repulsive and attractive interactions for long-range potentials.

Two regimes of interactions have been clearly identified:

(i) At low ionic strength ($[\mathrm{Cit}]_{\mathrm{free}} < 10^{-2}$ mol l^{-1}), electrostatic repulsion dominates the interparticle interactions and the phase behaviour is well described by the usual fluid–solid phase diagram of a repulsive system. The phase diagram of CitMF in the Π–Φ plane has been established and various iso-salinity lines have been plotted [13] allowing one to set the osmotic pressure of CitMF for a given ionic strength within the fluid domain. This regime of interactions is clearly the most useful for the synthesis of composite materials as it ensures CitMF stability. In this repulsive regime, a sample of CitMF remains a stable monophasic liquid for all intensities of magnetic field and magnetic field gradient.

(ii) For a higher ionic strength ($[\mathrm{Cit}]_{\mathrm{free}} > 10^{-1}$ mol l^{-1}), the interparticle potential is an attractive Lennard-Jones-like one and the phase behaviour of the magnetic fluid is well described by a phase diagram like for an atomic system, including gas–liquid transitions [19], the existence of a critical point [20] and fluid–solid transitions [21]. In particular, gas–liquid-like transitions have to be kept in mind when making composite materials, as they may appear if the ionic strength strongly increases locally in the material, even if the average ionic strength is low.

Between these two regimes, one goes smoothly from the repulsive to the attractive regime with increasing salinity. Knowledge of the phase diagrams in the different salinity regimes allows one to choose the best set of conditions (Π, Φ and I) for the precursor CitMF prior to the realization of a composite material.

2. Ferrofluids and polymer networks

When dealing with composites of polymers and ferrofluids, one commonly thinks about magnetic latexes used for biotechnological applications such as cell sorting. Most commercial products are based on polystyrene beads filled with magnetic particles dispersed thanks to a hydrophobic coating [7, 22]. About ten years ago, Zrínyi [2] introduced the opposite approach of using water-based polymers mixed with aqueous ferrofluids. The composite material obtained by associating a hydrogel and a ferrofluid has been called *a ferrogel*. The purpose was to obtain soft magnetic gels easily deformed by a magnetic field gradient (magnetostriction). The matrix was, for example, poly(vinyl-alcohol) cross-linked by glutaraldehyde and the magnetic materials consisted in magnetite grains (Fe_3O_4) about 10 nm in size dispersed in an acidic medium ($HClO_4$). Due to their high water content (more than 90 wt%!), ferrogels are much more deformable than magnetic latexes. Indeed, our own estimate of the Young modulus is about 10^4 Pa, which is two orders of magnitude lower than for classical rubbers. The goal of our study is to determine the influence of a charged ferrofluid properly dispersed in a polymer network on both the osmotic swelling equilibrium and the mechanical elasticity of the gel. We chose to mix a citrate-stabilized ferrofluid (CitMF) with acrylamide monomer (AM) that is polymerized and cross-linked in the pre-formed colloidal suspension. Acrylamide is polymerized thermally in the presence of a low amount of free radical initiator such as persulfate (peroxodisulfate) ions. Despite its simplicity, acrylamide is very useful for building a neutral hydrophilic network.

This section is organized as follows. In the first part, we describe the synthesis of ferrogels. The second and the third parts present mechanical and osmotic measurements respectively, with ferrogels of varying composition. Finally, we discuss possible interactions between ferrofluids and polymer networks that can explain the experimental data.

2.1. Synthesis

The cross-linker used was N, N'-methylene-bis-acrylamide (BA) and the initiator was ammonium persulfate (APS). Because APS is a 2:1 electrolyte that contributes to the ionic strength, the minimum possible concentration avoiding destabilization of the ferrofluid was used. The reactive mixture (2–3 ml) contained monomer (0.5 mol l^{-1} AM), cross-linker (5×10^{-4} or 2.5×10^{-4} mol l^{-1} for 1 or 0.5% BA/AM respectively), initiator (5×10^{-4} mol l^{-1} APS), tri-sodium citrate electrolyte (Na_3Cit) and ferrofluid (CitMF) at a volume fraction of magnetic nanoparticles denoted as Φ^0. The [Na_3Cit] concentration was either 5×10^{-3} or 8×10^{-3} mol l^{-1} for the two series of experiments which will be presented later in the text. The solution was degassed for 5 min before polymerization to eliminate oxygen. Then temperature was raised to 70 °C for 2 h to achieve completion of the reaction. Although the mixture had already gelled after 15 min, this long reaction time was used to ensure that we achieved about 96–98% of reacted monomer (measured yield). After careful removal, the ferrogels retained the cylindrical shape of the glass vessel (sample tube and Pasteur pipette for the swelling and the elasticity experiments respectively). After washing with deionized water to eliminate unreacted species, the ferrogels were immersed into a large volume of solution which was either pure water or a solution of Na_3Cit with a concentration ranging from 5×10^{-4} to 4×10^{-1} mol l^{-1}.

2.2. Elasticity measurements

Traditionally with hydrogels, the stress–strain measurements are performed in compression experiments on gel discs by using a tensile testing machine [23]. We preferred to use a home-

built set-up to apply a controlled elongation stress to ferrogels at equilibrium swelling, thereby visualizing their stretching directly. Moreover, our experiment has the advantage of keeping the sample in direct contact with the solvent. Of course, the Young modulus measured at low strain should be the same for elongation and compression experiments.

Long cylindrical samples of ferrogel were obtained by polymerizing the AM/CitMF mixtures in Pasteur pipettes of $d^0 = 5$ mm inner diameter and 50 mm length. The ferrogels were synthesized at different volume fractions Φ^0 of magnetic particles (from 1 to 7%) at a given ionic strength $[Na_3Cit]^0 = 8 \times 10^{-3}$mol l^{-1} as described in section 2.1 (*Synthesis*). The two extremities of the ferrogel cylinders were reinforced by polymerizing them at a higher cross-linker ratio (BA/AM = 5%) than the body of the ferrogel (BA/AM = 1%). In practice, the ferrogel was built in three steps corresponding to each section, added successively to the previous one while still freshly polymerized (at 10 min intervals). After polymerization, the ferrogels were carefully removed from the Pasteur pipettes. Special attention was paid to avoiding making any cracks in the bodies of the ferrogels, which could decrease their mechanical strength. Then they were allowed to swell in a solution at $[Na_3Cit] = 8 \times 10^{-3}$ mol l^{-1}. Once the swelling equilibrium was reached, the ferrogels were attached by their reinforced ends to two plastic nuts, the lower one static, the upper one mobile, and connected to the arm of a counterweight balance. The system was immersed in a transparent reservoir containing an aqueous solution of citrate salt at $[Na_3Cit] = 8 \times 10^{-3}$ mol l^{-1}, thus enabling direct observation of the coloured ferrogel under extension with a video camera mounted with a 75 mm zoom lens.

The stress was applied by loading the pan of the balance with calibrated weights ($M = 10$ g maximum). We checked that both ends of the sample were held firmly and without sliding by the nuts during the whole elongation test. The axial dimension L of the ferrogel was recorded from the initial state under zero load L_0 up to a maximum elongation state always below rupture. Usually a change of the load is followed by mechanical oscillations. Therefore a delay of 1 min between two consecutive measurements was always respected to achieve static equilibrium of the sample.

The strain is defined as

$$\varepsilon = \frac{L - L_0}{L_0}$$

where L_0 is the length of the gel between the two anchoring points in the unloaded state (see figure 1(a)) and L is the length when a weight M is placed on the pan of the balance. The cross-section area of the cylinder is denoted as A_0 under zero load and A under a non-zero load. Assuming a constant volume of the sample under deformation, we have $A = A_0/(1 + \varepsilon)$. We deduce the true stress acting on the gel loaded with a weight M:

$$\sigma = \frac{Mg}{A_0}(1 + \varepsilon)$$

where $g = 9.8$ m s^{-2} is the gravity constant. Depending on the degree of swelling, the diameter d of each cylindrical sample after swelling and before stretching ranges between 6.5 and 8.5 mm. The plots in figure 1(b) represent the strain–stress measurements for ferrogels at the same polymer and cross-linker concentrations but with varying volume fractions of nanoparticles Φ^0 during the synthesis. We observe no significant deviation of the curves from linearity, indicating that the ferrogels exhibit a rubber-like elasticity over the whole domain of deformation studied here.

The Young modulus E is simply given by the slope of σ versus ε and can be plotted as a function of Φ^0 (figure 1(c)). These data show that the mechanical strength of the ferrogels increases significantly with the volume fraction of the inorganic nanoparticles introduced

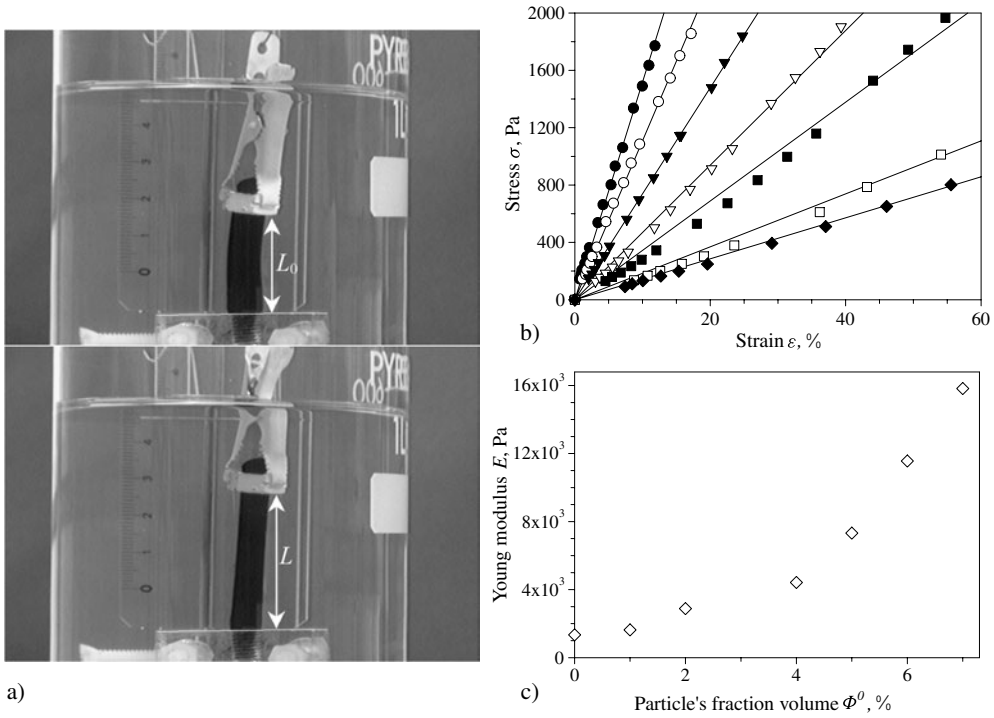

Figure 1. (a) The stretching experiment on a ferrogel in the swollen state ($\Phi^0 = 4\%$) under a controlled load ($M = 0$ g for the upper picture, $M = 5.4$ g for lower picture). (b) Strain–stress curves obtained at constant cross-link density BA/AM = 1% and [AM] = 0.5 mol l^{-1} during synthesis with increasing particle volume fraction $\Phi^0 = 0\%$ (filled diamonds), 1% (empty squares), 2% (filled squares), 4% (empty triangles), 5% (filled triangles), 6% (empty circles) and 7% (filled circles). All these ferrogels were prepared and swollen in solutions where $[Na_3Cit] = [Na_3Cit]^0 = 8 \times 10^{-3}$ mol l^{-1}. (c) The elastic modulus E of the ferrogels measured from the slopes of the strain–stress curves plotted as a function of the particle volume fraction Φ^0 during synthesis.

during preparation. Therefore ferrogels can be considered as composite materials where the polymer matrix is reinforced by the solid component. However, the elastic modulus remains around 10^4 Pa, which is still two orders of magnitude lower than usual values for elastomers ($E \sim 10^6$ Pa).

2.3. Swelling and release

The ferrogels were allowed to reach their swelling equilibrium in Na_3Cit for approximately three weeks. The immersion bath was changed several times in order to get rid of free particles that were not trapped within the ferrogel. The swollen ferrogel at equilibrium was weighted (m_{swollen}) and then dried at 70 °C to also obtain its dry weight (m_{dry}). Finally, the iron content remaining in the dried ferrogel was measured by atomic absorption spectroscopy with a hollow cathode lamp in a Perkin-Elmer AAnalyst 100 apparatus. Thus we can calculate the mass of iron oxide ($m_{Fe_2O_3}$) remaining after release of some of the magnetic particles and compare it to the mass of maghemite initially introduced in the ferrogel during the synthesis ($m^0_{Fe_2O_3}$). Two

ratios are defined from those experimental measurements:

$$Q = \frac{m_{H_2O}}{m_{polymer}} = \frac{m_{swollen} - m_{dry}}{m_{polymer}} \qquad \text{and} \qquad R = \frac{m^0_{Fe_2O_3} - m_{Fe_2O_3}}{m^0_{Fe_2O_3}}.$$

Q is the degree of swelling commonly used for hydrogels defined as the amount of water m_{H_2O} absorbed by the gel normalized by the weight of polymer network $m_{polymer}$. The water content m_{H_2O} is given by the difference in weight between the swollen gel and the dry gel. Please note that in the case of ferrogels, the dry weight consists of polymer, particles and citrate salt taken together. Only the mass of polymer, $m_{polymer}$, thus has to be computed from the initial concentration of monomer assuming a yield of 100%. The amount of water in the synthesis vessel being known precisely, an initial value of the swelling ratio is calculated. This Q^0-value ranges from 25 to 27 depending on the volume fraction Φ^0 of solid iron oxide. R is the release parameter specific to ferrogels that we define as the fraction of magnetic particles which are not trapped by the ferrogel and are released in the swelling bath.

We performed two series of swelling experiments with ferrogel samples:

- We varied the volume fraction Φ^0 of magnetic particles at preparation from 1 to 9% while we kept the ionic strength at a low value identical in the swelling bath and during synthesis $[Na_3Cit] = [Na_3Cit]^0 = 8 \times 10^{-3}$ mol l^{-1}. For this series, the cross-linker ratio BA/AM was 1%. The measurements of Q and R versus Φ^0 are presented in figure 2.
- For a given volume fraction $\Phi^0 = 3.8\%$, we kept the citrate concentration at preparation constant: $[Na_3Cit]^0 = 5 \times 10^{-3}$ mol l^{-1}, but we increased the ionic strength $[Na_3Cit]$ in the swelling bath from 0 to 0.4 mol l^{-1}. The cross-linker ratio BA/AM was 0.5% for all of those samples. Figure 3 compares the swelling Q of ferrogels prepared at $\Phi^0 = 3.8\%$ to the case for undoped hydrogels ($\Phi^0 = 0\%$) swollen at various concentrations of citrate. The release R of the magnetic content is plotted in figure 3 as a function of $[Na_3Cit]$ on a secondary axis.

Although the degrees of cross-linking are different for the two series of experiments, they remain in the regime of low cross-link density, where the elastic modulus of the hydrogels grows linearly with the ratio BA/AM. Only at higher cross-linker ratio (above 2%) and higher polymer concentration do hydrogels start to exhibit a heterogeneous distribution of chemical nodes concomitant with a maximum of their shear modulus [24].

2.3.1. The role of the initial particle volume fraction. In figure 2, we observe that the swelling Q decreases continuously as a function of the volume fraction Φ^0 of magnetic particles in the ferrogel during polymerization. For the higher content of particles ($\Phi^0 = 9\%$), we see that $Q = 20$ becomes smaller than the initial water content after synthesis $Q^0 = 25$, which means that the ferrogel actually contracted slightly in the swelling bath. As regards the release, we note that the network systematically lost a large fraction of the particles present at preparation ($R = 35$–45%, except for the lower values of Φ^0 where $R \sim 15\%$). In other words, *more than half of the particles were efficiently trapped in all cases.*

2.3.2. The role of the ionic strength during swelling. In figure 3, the case of the undoped hydrogel and of the ferrogel, both prepared in $[Na_3Cit]^0 = 5 \times 10^{-3}$ mol l^{-1} then swollen in pure water, is of particular interest because the corresponding values of the swelling are far above the rest of the plot: $Q = 308$ and 78.5 for $\Phi^0 = 0$ and 3.8% respectively. For the other samples immersed in a non-zero citrate concentration, we observe a different variation of Q versus $[Na_3Cit]$ for iron-oxide-loaded ferrogels and unloaded hydrogels. Without

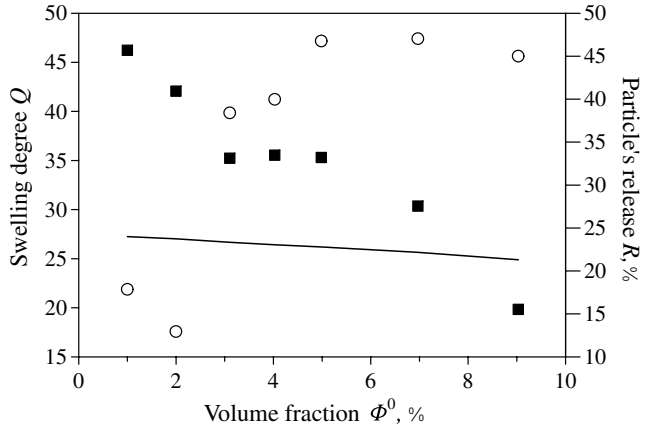

Figure 2. The swelling ratio Q (filled squares) and the particle release R (circles) versus the volume fraction Φ^0 of magnetic particles in the preparation mixture. The solid line represents the swelling ratio at preparation Q^0, which varies from 27 to 25 depending on Φ^0. All of these ferrogels were prepared and swollen at low salinity $[Na_3Cit] = [Na_3Cit]^0 = 8 \times 10^{-3}$mol l^{-1} and their cross-link ratio was always BA/AM = 1%.

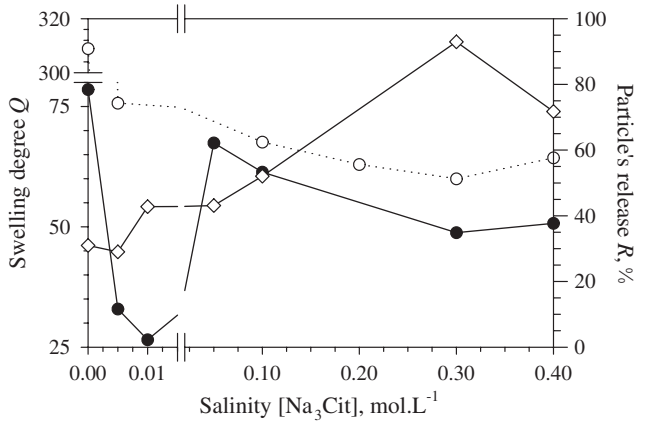

Figure 3. The degree of swelling Q (filled circles) and the particle release R (diamonds) versus sodium citrate concentration [Na_3Cit] in the swelling bath for ferrogels prepared with a volume fraction of magnetic particles $\Phi^0 = 3.8\%$ and for undoped hydrogels (empty circles). For all those ferrogels, the cross-link ratio was BA/AM = 0.5% and the swelling ratio at preparation $Q^0 = 27$. For visualization purposes, the horizontal scale is dilated in the region of low salinity ($<10^{-2}$ mol l^{-1}) and the vertical axis is broken to represent the first point concerning the hydrogel, which is far above the other ones ($Q = 308$).

particles, the swelling Q decreases smoothly as a function of salinity, then saturates to a value $Q \sim 65$, which is still twice larger than $Q^0 = 27$. The plots look different for ferrogels. They exhibit a minimum value of Q near the concentration $[Na_3Cit] = 1 \times 10^{-2}$ mol l^{-1}, which is followed by a maximum of Q located around 5×10^{-2} mol l^{-1} for $\Phi^0 = 3.8\%$. After this maximum, the swelling reaches a plateau value $Q \sim 50$ for $\Phi^0 = 3.8\%$, smaller than the plateau $Q \sim 65$ for the unloaded hydrogel. Starting from $R \sim 30\%$ at the lowest salt concentration $[Na_3Cit] = 5 \times 10^{-3}$ mol l^{-1}, R rises significantly for higher citrate salt concentrations for the ferrogels initially loaded at $\Phi^0 = 3.8\%$. In that case, a maximum of

Figure 4. Observation by optical microscopy of the gas–liquid-like transition inside ferrogels prepared at an initial particle volume fraction $\Phi^0 = 3.8\%$ and a degree of cross-linking BA/AM = 0.5% swollen in a salt concentration $[Na_3Cit] = 0.25$ mol l^{-1}: (a) 9 h after the beginning of swelling; (b) after 9 h of swelling and application of a magnetic field of 1 T for 10 min; (c) after 24 h of swelling. The bar length is 50 μm. The dark background is due to the light absorption spectrum of ferric oxide. The dots are microdroplets concentrated in particles (mentioned in the text as 'liquid-like' phase).

(This figure is in colour only in the electronic version)

particle release $R = 93\%$ is reached for 0.3 mol l^{-1} citrate. This loss of particles is twice as large as for the ferrogel at approximately the same initial load $\Phi^0 = 4\%$ but swollen in $[Na_3Cit] = 8 \times 10^{-3}$ mol l^{-1} instead (figure 2). All these features of the curves will be discussed in section 2.4 (*Interpretation*).

2.3.3. Particle destabilization at high salinity. In the first part of this paper, we have seen that the citrate concentration is a control parameter in the phase diagram of ferrofluids, the other parameter being the volume fraction. This series of ferrogels at varying salinity is also chosen to explore possible shifts of the boundaries of the phase diagram when the colloidal particles are dispersed in a polymer matrix rather than in a pure solvent. All of the ferrogels at $\Phi^0 = 3.8\%$ were prepared from the same CitMF ferrofluid characterized by a size distribution with modal diameter $d_0 = 9$ nm and $\sigma = 0.25$. In the ferrofluid at $\Phi^0 = 3.8\%$ volume fraction (without polymer), the gas–liquid transition mentioned in section 1.2 of this paper occurs at $[Na_3Cit] = 0.19$ mol l^{-1}. Above this threshold concentration, the continuous gas-like phase coexists with micron-sized droplets of a liquid-like phase, which is more concentrated in particles. The same phase separation of the particles was also observed by optical microscopy in the ferrogels prepared at $\Phi^0 = 3.8\%$ and swollen in Na_3Cit above a threshold concentration of 0.25 mol l^{-1} (figure 4). At this salt concentration, the ferrogel looked homogeneous during the first hours of swelling (figure 4(a)). However, the application of a strong magnetic field (1 T) initiated a visible roughness of the sample (figure 4(b)). After a longer time in the swelling bath, the sample became clearly phase separated, as droplets concentrated in particles had appeared (figure 4(c)). Being embedded in the polymer matrix, these droplets neither elongate nor form chains when a magnetic field is applied, unlike in the normal case of a fluid CitMF.

2.4. Interpretation

When the polymerization of BA/AM is achieved in the presence of CitMF, all the magnetic particles initially introduced are located inside the polymer network because all the reactive mixture has gelled (despite a negligible volume of liquid supernatant). Hence the volume fraction of particles in the ferrogel is initially equal to Φ^0 as in the liquid mixture. As soon

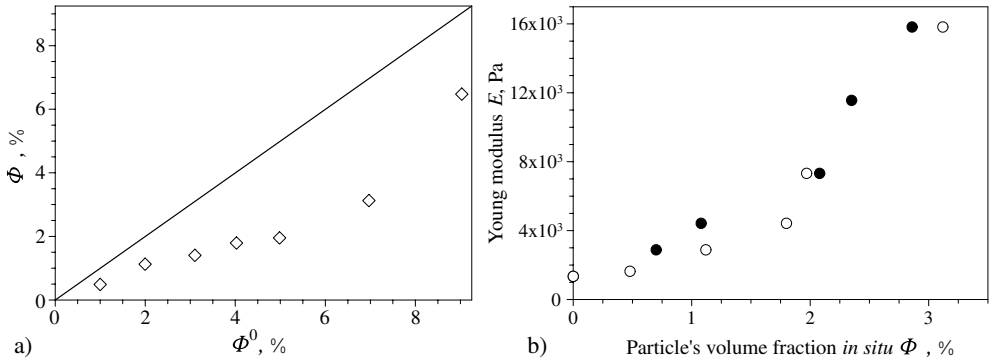

Figure 5. (a) The final particle volume fraction in the swollen ferrogel Φ as a function of the initial volume fraction Φ^0 during synthesis computed from the conservation equation with the data of figure 2. (b) The elastic Young modulus from the data of figure 1(c) plotted versus the actual particle volume fraction Φ calculated from Q and R where Q either comes from weight measurements (open circles) with the samples presented in figure 2 or is estimated from the relative increase of diameter (filled circles) using $Q/Q^0 = (d/d^0)^3$ for the samples used for the elongation tests plotted in figure 1. All of these ferrogels were prepared at BA/AM = 1% and $[Na_3Cit]^0 = 8 \times 10^{-3}$ mol l^{-1}.

as the ferrogel is plunged into the swelling bath, this volume fraction of particles starts to decrease. The particle concentration after some time in the swelling bath is equal to Φ, which is less than Φ^0 due to two phenomena occurring simultaneously. On the one hand, the ferrogel exhibits a significant volume increase due to water absorption by the polymer. This 'inflation' contributes to dilution of the particles by a factor Q_0/Q. On the other hand, a fraction R of the particles have been released into the external solution during the swelling process. Thus a fraction $(1 - R)$ remains in the swollen ferrogel. Therefore we can estimate the volume fraction of particles in a state characterized by a release fraction R and a swelling ratio Q by using a simple conservation law:

$$\Phi = \Phi^0(1 - R)\frac{Q^0}{Q}.$$

We notice an important difference between the first series of experiments at low citrate concentration and the second series where this salt concentration was varied from low to high values. In the low-salinity case, the ferrogel always reached a static state where the weight of the ferrogel did not vary any longer and the release of iron oxide in the outer solution stopped. Thus the particle volume fraction Φ had reached an equilibrium value. In the series of experiments with varying salt concentration during swelling, we noticed for some high-salinity cases that the release never stopped even though the weight of the swollen ferrogel was constant. In particular, this absence of equilibrium occurred for the initial particle volume fraction $\Phi^0 = 3.8\%$ and for citrate concentrations around the destabilization threshold at 0.25 mol l^{-1}. Therefore we comment on the two types of experiment separately.

The role of the particle volume fraction Φ^0 at low sodium citrate concentration, identical during synthesis and swelling, $[Na_3Cit] = [Na_3Cit]^0 = 8 \times 10^{-3}$ mol l^{-1}. Although it is calculated rather than measured *in situ* by an independent experiment, this estimate of the volume fraction Φ leads us to make the following statement: *the greater the number of particles that we introduced in the synthesis, the more concentrated the ferrogel that we got after the swelling and release equilibration.* This result is not trivial because the increase of the release

fraction R for increasing values of Φ^0 (see figure 2) tends to diminish Φ, while the decrease of the swelling ratio Q produces the antagonist effect. The effect of Q is stronger than the effect of R because in the end, Φ increases when Φ^0 increases. Realized for the same low citrate concentration, the mechanical elongation test with a series of ferrogels at increasing Φ^0 shows that the rigidity of ferrogels also increases continuously with the solid volume fraction at preparation Φ^0. In figure 5(b), we plot the measured values of the Young modulus as a function of the estimate of the actual particle volume fraction Φ in the swollen ferrogels. There were two ways to compute those values of Φ. The conservation law states that Φ/Φ^0 is the product of Q^0/Q and $(1 - R)$. The ratio of the degree of swelling Q to its value Q^0 right after synthesis can be either computed from the weight measurements or estimated geometrically by measuring the relative change of diameter of the cylindrical samples (assuming an isotropic swelling):

$$\frac{Q}{Q^0} = \left(\frac{d}{d^0}\right)^3$$

Even though they were applied to two different series of samples, the two methods used to compute Φ give similar results for the plot of E versus Φ. Thus we can deduce that the elastic strength of the ferrogels studied increases almost linearly with the volume fraction of solid particles in the swollen state. The nanoparticles can thus be considered as reinforcement fillers.

Coming back to the decrease of the degree of swelling Q as a function of the particle volume fraction Φ^0 (figure 2), we can explain this behaviour by the mechanical reinforcement of ferrogels compared to the undoped hydrogel. In the standard Flory–Rehner theory of hydrogel swelling, indeed, the degree of swelling Q is determined by a competition between the osmotic pressure of the polymer which is the driving force for water absorption and the elastic energy resisting network deformation due to volume increase [25]. More precisely, the degree of swelling scales with the Young modulus like $Q \propto E^{-3/5}$ in the limit of high Q-values. Usually this law is tested for rubbers by varying the cross-link density. Here with ferrogels we varied the concentration of entrapped particles instead. We find a semi-quantitative agreement between our measurements and the theory of swelling, because Q and E are respectively a decreasing and an increasing function of the particle volume fraction Φ in the swollen state. In other words, *the limitation of ferrogel swelling by the particles is due in part to a mechanical reinforcement.*

The variation of the ionic strength $[Na_3Cit]$ *in the swelling bath for a given salinity during synthesis,* $[Na_3Cit]^0 = 5 \times 10^{-3}$ *mol* l^{-1}*, for undoped hydrogels and ferrogels at* $\Phi^0 = 3.8\%$. The variation of the swelling ratio Q with the [Na_3Cit] concentration in the swelling bath is rather complicated (figure 3). Poly(acrylamide) hydrogels are indeed neutral networks and thus are supposed to be insensitive to the effect of charge screening by an external electrolyte. We report here two effects of the tri-sodium citrate electrolyte, both on undoped hydrogels and on ferrogels. On the one hand, the presence of citrate during polymerization increases the swelling in pure water and leads to an influence of [Na_3Cit] on the swelling ratio even for undoped hydrogels. On the other hand, the differences in swelling between the ferrogels and the undoped hydrogel taken as the reference demonstrate the influence of citrate on the particle's interactions, stability and release.

- *The influence of citrate on network swelling.* When prepared in $[Na_3Cit]^0 = 5 \times 10^{-3}$ mol l^{-1} and swollen in pure water, a hydrogel containing no particles or particles at $\Phi^0 = 3.8\%$ absorbs a much larger quantity of water ($Q = 308$ and 78.5 respectively) than when swollen in any concentration of salt. This enhancement of the swelling is reminiscent

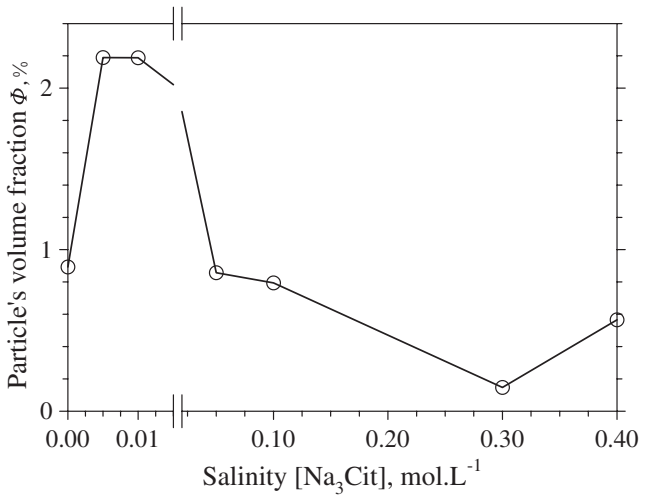

Figure 6. The final particle volume fraction in the swollen ferrogel Φ as a function of the tri-sodium citrate concentration [Na_3Cit] in the swelling bath, computed from the measurements of Q and R represented in figure 3. For visualization purposes, the horizontal scale is dilated in the region of low salinity ($<10^{-2}$ mol l^{-1}). All ferrogels were prepared at BA/AM = 0.5% and $[Na_3Cit]^0 = 5 \times 10^{-3}$ mol l^{-1}.

of the polyelectrolyte effect obtained with charged super-absorbent hydrogels [26]. Ionization of poly(acrylamide) has been reported in the literature, but only at pH higher than 12 [27], which is not the case here because tri-sodium citrate is a pH 7 buffer. Thus we can only conclude that some unidentified electrostatic charges are present on the polymer backbone in our conditions of polymerization. When tri-sodium citrate is also present in the swelling solution, the swelling ratio of the undoped hydrogel decreases slightly from $Q \sim 75$ for $[Na_3Cit] = 5 \times 10^{-3}$ mol l^{-1} to $Q \sim 65$ for $[Na_3Cit] = 4 \times 10^{-1}$ mol l^{-1}. This variation is low enough for one to consider that the residual charges of the network are screened for all electrolyte concentrations used during swelling. In the following, we use this curve of Q versus [Na_3Cit] for the bare hydrogel as the reference level for discussing the influence of the particles.

- *The influence of citrate on the interactions, stability and release of particles.* The difficulty of addressing the issue of the osmotic role of particles during the swelling of ferrogels arises from the particle release, which varies a lot as a function of the ionic strength (figure 3). Therefore the particle volume fraction is far from constant when salinity is varied. Nevertheless, this concentration of particles in the swollen state of the ferrogel can be estimated from the measurements of Q and R and the conservation law (figure 6).

Two domains of salinity can clearly be identified, corresponding to two regimes of interactions between the particles and the polymer network:

(a) *Low salinity* $[Na_3Cit] < 1 \times 10^{-2}$ mol l^{-1}. Apart from the case of pure water where the particles are diluted by the strong water absorption, the volume fraction of entrapped particles remains constant and approximately equal to $\Phi = 2.2\%$ over this whole range of salinity (figure 6). Thus we can really discuss the osmotic contribution of particles to the network swelling at a constant Φ. In this range of ionic strength, the swelling of the undoped hydrogel is always larger than the swelling of the ferrogel, as shown in the left part of figure 3. This low-salinity regime corresponds to strong electrostatic

repulsions between the particles associated with a high osmotic pressure of the ferrofluid. It also corresponds to a strong osmotic pressure of the hydrogel, as the latter swells more in this regime than in the domain of high ionic strength. Nevertheless, comparing the swelling of the hydrogel and that of the ferrogel, the degree of swelling of the latter is noticeably lower. This indicates that *the osmotic pressure of the composite is smaller than the osmotic pressure of the hydrogel* and therefore smaller than the sum of the osmotic pressures of the two components individually. From this negative cross-term in the total osmotic pressure, we can conclude that attractive interactions between the polymer and the particles exist.

The adsorption of polyacrylamide chains on ferric oxide surfaces was indeed reported in the literature [28]. This hypothesis of a (weak) binding between particles and network is also supported by the efficient entrapment of a fraction $(1 - R)$ of the nanoparticles while the remaining ones (R) escape from the ferrogel. One may wonder what the processes at the microscopic scale leading to this partial entrapment are. The kinetics must be limited by the diffusion of the nanoparticles through the pores of the polymer network. The volume increase caused by water swelling enlarges the polymer mesh size and liberates particles that were initially trapped. However, the swelling does not completely wash out the particles. The remaining particles cannot leave the ferrogel once the release equilibrium is attained, which means that the particles are not free to diffuse in the polymer network. Thus the immobilization of a large fraction of particles is neither simply due to steric hindrance nor due to the slow kinetics of diffusion. Therefore an attractive interaction must exist between the polymer chains and the iron oxide nanoparticles.

(b) *High salinity* $[Na_3Cit] > 1 \times 10^{-1}$ mol l^{-1}. We know from past studies with CitMF ferrofluids that the sign of the second virial coefficient changes from positive (repulsion) to negative (attraction) at a citrate concentration of about 1×10^{-1} mol l^{-1} [13]. For this salinity, the particles behave like an ideal gas. Above this threshold, the osmotic pressure of a ferrofluid at constant volume fraction and increasing ionic strength decreases because the interparticle potential becomes more and more attractive.

For particles embedded in a ferrogel, we observe that the swelling at $[Na_3Cit] = 1 \times 10^{-1}$ mol l^{-1} is approximately the same for a blank hydrogel ($Q = 68$) and a ferrogel prepared at $\Phi^0 = 3.8\%$ ($Q = 61$). At this salt concentration and above, the discrepancy between the degrees of swelling of the ferrogel and of the hydrogel existing in the regime of low salinity has almost disappeared, even though a gap remains between the Q-levels for the hydrogel and the ferrogel. At the same time, the particle release fraction R increases strongly with the ionic strength (figure 3). The estimate of the particle volume fraction (figure 6) indeed shows a deep decrease down to a minimum $\Phi = 0.15\%$ at $[Na_3Cit] = 3 \times 10^{-1}$ mol l^{-1}. Being more dilute and having their electrostatic repulsions screened by the electrolyte, the nanoparticles on their own must have a much lower osmotic pressure than at low ionic strength. Their negative contribution to the osmotic pressure of the composite also disappears, as seen from the much larger swelling of the ferrogels in the salinity range 5×10^{-2}–3×10^{-1} mol l^{-1} as compared to the low-salt domain 5×10^{-3}–1×10^{-2} mol l^{-1}. This feature is the signature of the decrease of the supposed attractions between the particles and the polymer network when the ionic strength increases.

In spite of the previous statement, we cannot conclude that the polymer becomes totally 'transparent' for the interactions between particles at high ionic strength. The study of particle destabilization shows indeed that the threshold ionic strength for gas–liquid-like phase separation is shifted toward a higher salinity in the ferrogel prepared at $\Phi^0 = 3.8\%$ compared to the ferrofluid at the same volume fraction ($[Na_3Cit] = 0.25$ and 0.19 mol l^{-1}

respectively). This observable shift of the boundary in the phase diagram is not simply caused by the lower volume fraction in the ferrogel as compared to the ferrofluid, because it occurred after a time lapse of about 24 h (figure 4), much lower than the waiting time before the measurements of figure 3 (three weeks), so the ferrogel was still concentrated in particles at that time. Therefore this shift of the onset of phase separation shows that *the polymer network somehow hampers the attractive interactions between particles*. Moreover, the decrease of particle release R at 0.4 mol l^{-1} compared to its maximum at 0.3 mol l^{-1} can be explained by a larger amount of the liquid-like phase. The high viscosity of this concentrated phase certainly causes a kinetic blockage of further particle release (please recall that no real equilibrium of particle release was reached for the two highest values of the ionic strength).

2.5. Conclusions

This study has shown the possibility of including charged magnetic nanoparticles in a polyacrylamide hydrogel, while maintaining repulsive interactions between the particles. The advantage of polymerizing the hydrogel directly in a stable colloid (CitMF) consists in realizing a homogeneous dispersion of nanoparticles without clusters. The main control parameter determining the entrapment of particles in the polymer matrix and the degree of swelling is shown to be the ionic strength during swelling. We were indeed able to obtain swollen ferrogels at final particle volume fractions up to $\Phi = 6.5\%$ at low ionic strength (8×10^{-3} mol l^{-1}) and $\Phi = 2.2\%$ at a larger ionic strength (5×10^{-2} mol l^{-1}). We identified two different effects of the particles on the water absorption by the ferrogel. On the one hand, the swelling of the network Q is limited by the increase of the stretching modulus E, which is proportional to the volume fraction Φ of particles behaving as hard fillers. On the other hand, at constant Φ, we noted that the degree of swelling Q is also limited by a decrease of the osmotic pressure of the composite ferrogel compared to the osmotic pressure of the hydrogel alone. This negative cross-term is attributed to an attraction between the particles and the polymer network, which still needs to be clarified (coordination bonds between the amide moieties of the monomer and the ferric cations).

The reducing of this interaction between the polymer and the inorganic colloids when salt concentration increases is responsible for the minimum of the curve of Q versus [Na_3Cit] for the ferrogel in figure 3. Such a minimum of the swelling ratio as a function of salinity has been reported for polyampholite hydrogels, which are made of copolymers bearing both positive and negative charges [29]. Therefore ferrogels and polyampholites are analogous in the sense that the network is subjected to a combination of attractive and repulsive interactions, which are both screened by the ionic strength. A last point remaining to be completely addressed is the mechanism by which tri-sodium citrate can induce the presence of charges on the polyacrylamide chains during polymerization. This residual charge of polyacrylamide networks can be estimated to a few per cent of monomers or less. When prepared in a tri-sodium citrate solution, a hydrogel swollen in pure water absorbs a large quantity of water ($Q \sim 300$), but this value is still lower than for a real polyelectrolyte hydrogel made of a copolymer of AM and 10 mol% of negatively charged sodium acrylate (SA): in that case the swelling is even higher ($Q \sim 1000$ for 10% of charged comonomers; data not shown).

Finally, the most direct practical application of ferrogels consists in their macroscopic response to a magnetic field or field gradient. Different configurations can be imagined to test the properties of 'magnetoelastics'. Recently the enhancement of the Young modulus by application of a magnetic field was demonstrated in a stretching geometry with a sample made of a magnetic powder and a silicone rubber [30]. This strengthening under a magnetic field

was also reported in a compression experiment with a poly(vinyl-alcohol)-based ferrogel and attributed to a demagnetizing effect of the cylindrical sample [31]: the compression modulus increases (decreases) under an applied field perpendicular (parallel) to the cylinder axis. The variation would be quite the opposite for the elongation modulus. Our ferrogels are very promising for use in such magnetoelastic experiments, because their elastic modulus remains low (maximum $E = 1.6 \times 10^4$ Pa for a relatively high magnetic load $\Phi = 6.5\%$).

3. Composite suspensions of laponite discs and maghemite spheres: probing a colloidal system with another one

Laponite is a synthetic clay of general formula $Si_8M_{g5,45}Li_{0,4}H_4O_{24}Na_{0,7}$. The particles are discotic (diameter around 30 nm, thickness of 1 nm) and make stable suspensions when dispersed in aqueous media for convenient conditions of pH ($9 < \mathrm{pH} < 10.5$: below pH 9, the magnesium ions dissolve in solution; above pH 10, dissolution of silica appears) and ionic strength (if the ionic strength is higher than 2×10^{-2} mol l^{-1}, attractions in the system lead to flocculation). For these experimental conditions, particles are chemically stable and have a negative average surface charge.

For ionic strength ranging between 10^{-4} and 2×10^{-2} mol l^{-1}, laponite suspensions exhibit a rheological transition over a given volume fraction range, the nature of which is still a subject of debate [32–37]. The transition is related to the appearance of a pseudoplateau in the equation of state of the system and the end of the pseudoplateau may be related to an ill-defined isotropic–nematic transition [38]. Although this pseudoplateau in the equation of state could be associated with a first-order transition, the laponite suspensions stay macroscopically homogeneous and the existence of biphasic samples has never been reported. The hypothesis of an isotropic–nematic transition that occurs on a microscopic scale because of long-range electrostatic interactions preventing the system from exploring the whole phase space can be formulated.

We have tested this hypothesis in [14] by including maghemite nanoparticles (CitMF) as probes in laponite suspensions in order to determine their spatial repartition for different Φ_{laponite} covering all parts of the laponite equation of state. Citrate-coated maghemite particles were the best candidates for being probes as they have magneto-optical properties allowing local viscosity measurements [9]. They are spherical, with a size similar to that of laponite particles; they have the same counterions as laponite (Na^+) and can be dispersed in the same conditions of pH and ionic strength as laponite. They have a neutron scattering length density that is very different from that of laponite particles, thereby allowing a good contrast for SANS experiments.

3.1. Including probes in laponite suspensions

The suspensions including probes were obtained by stirring laponite particles (purchased from Laporte Industries Ltd) in a suspension of maghemite particle probes at $\Phi_{\mathrm{probes}} = 0.05\%$ with $Na_3Cit = 2.5 \times 10^{-3}$ mol l^{-1} and $NaOH = 10^{-4}$ mol l^{-1} to set pH 10. The citrate concentration was above the critical concentration for citrate desorption and corresponded to an ionic strength of 1.5×10^{-2} mol l^{-1} below the destabilization threshold of laponite suspensions. The volume fraction of probes was kept constant at a very small value (0.05%) to avoid disturbing the laponite suspensions. Suspensions were left to stand for ten days before performing any measurements.

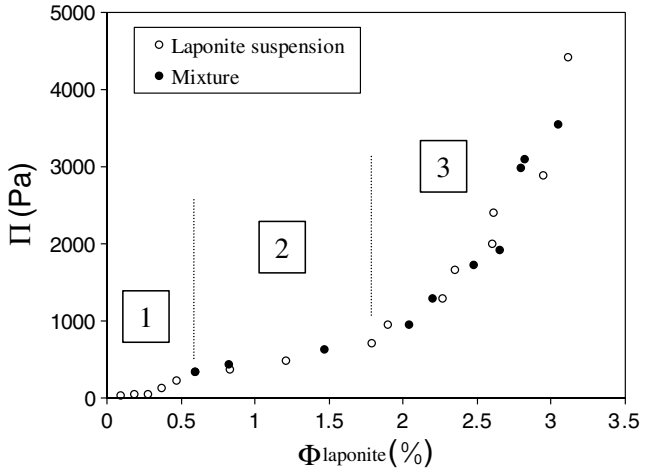

Figure 7. The experimental state isotherm curve Π versus Φ for pure laponite suspensions in a Na_3Cit solution (2.5×10^{-3} mol l^{-1}) at pH 10 (open dots) and for laponite doped with maghemite probes in the same chemical conditions (filled dots). The dotted lines separate the three characteristic domains of the equation of state considered in the text (before, along and after the pseudoplateau) [14].

3.2. The equation of state of the mixture

The inclusion of the probes did not shift the fluid/solid transition and did not modify the equation of state of the laponite suspensions, as can be seen in figure 7 which represents the osmotic pressure as a function of the volume fraction either with or without the probes, by analogy with the pressure–density isotherms for van der Waals gases. This curve has been obtained by direct measurements of Π with a membrane osmometer for the lowest volume fractions and by osmotic compression (where Π is controlled by a solution of dextran) for the highest ones. For this latter experiment, the constant parameter is not Φ_{probes} but the ratio $\Phi_{\text{probes}}/\Phi_{\text{laponite}}$. This ratio ensures that Φ_{probes} stays in the range 0.05 to 0.4% and the osmotic pressure of maghemite particles remains below 45 Pa (see section 1) which is far below that for laponite suspensions. Laponite particles thus set the osmotic pressure of the hybrid system to pre-determined values.

The pseudoplateau of the equation of state still exists for the composite dispersion. Neither its border nor its value were shifted. The three parts of the equation of state (before, along and after the pseudoplateau) will be denoted hereafter as parts 1, 2 and 3 respectively. This result indicates that the inclusion of a few maghemite particles changes neither the interactions nor the structure of the system. These maghemite particles can indeed be considered as non-invasive probes.

3.3. Probing laponite gel heterogeneity, using magneto-optical probing and SANS

Particles have an intrinsic optical anisotropy, such that CitMF becomes birefringent when subjected to a magnetic field as particles orientate along the field. The measurement of temporal birefringence relaxation after the application of a magnetic pulse (0.017 T) enables one to measure a relaxation time τ for the probes, which is characteristic of their rotational diffusion. Knowing the diameter of the particles (from magnetic measurement) and using the Stokes–Einstein relation, the viscosity of the mixture in the vicinity of the probes can be attained by such a measurement [9].

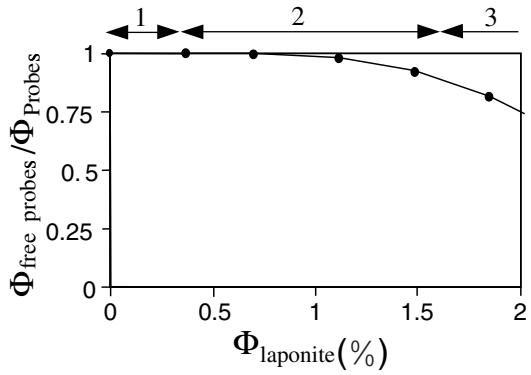

Figure 8. The ratio of the free maghemite probes in mixtures when increasing the volume fraction of laponite particles. The three domains correspond to the three regions of the equation of state [14].

It appeared that this time τ is comparable for maghemite particles in water and in laponite whatever the value of $\Phi_{laponite}$, except for region 3 of the equation of state where τ is shorter. This shows that the particle's dynamics is not slowed down in the region of the pseudoplateau even though the suspensions are solid. In addition, no aggregates are formed, as they would increase the relaxation time. The ratio between the birefringence in solid suspensions and in the solution for the same volume fraction of maghemite particles gives the percentage of freely rotating particles at 0.017 T and is presented in figure 8. It departs smoothly from 1 in the middle of the pseudoplateau to reach 0.75 in the region of the state isotherm curve 3. Thus some probes begin to be mechanically blocked only at the end of the pseudoplateau and become more and more numerous, although laponite suspensions are solid from the beginning of the plateau. This result is in good accord with the hypothesis of microscopic heterogeneities in laponite gels, liquid pockets coexisting with solid domains.

The spatial repartition of the maghemite probes is studied by SANS. In these experiments, the solvent was a H_2O/D_2O mixture, whose neutron scattering length density exactly matches the value for laponite particles. Indeed, the measured intensity only comes from the contribution of maghemite particles. The perfect extinction of laponite enables one to get an effective structure for the probes. It is obtained by dividing absolute intensities by the form factor of the maghemite particles in dilute solution in pure solvent. The scattering vector ranged from 1.6×10^{-3} Å^{-1} to 3×10^{-2} Å^{-1}. It appeared that at low $\Phi_{laponite}$, the structure factor is close to one (section 1), indicating that the probes are homogeneously distributed. Along the pseudoplateau of the Π versus $\Phi_{laponite}$ plot, the effective structure factor increases a lot with $\Phi_{laponite}$ at small q, revealing an increasing heterogeneity. This suggests that the probes are located in liquid-like pockets. In other words, they are excluded from the dense regions where laponite particles are localized and share strong attractions. When $\Phi_{laponite}$ increases, the size of these large solid-like clay domains grows, while liquid pockets shrink and the effective structure factor increases further. For the largest $\Phi_{laponite}$ (section 3), the structure factor decreases again and even shows a pronounced depletion at low q. The probes are again homogeneously dispersed with laponite, but the presence of laponite particles filling all the space prevents the probes from localizing and moving freely.

Thus SANS results are in agreement with local mechanical measurements and allow one to give an illustration of a hybrid system for the different parts of the equation of state (figure 10). This was possible because, first, the chemical conditions of the mixture have been found and, second, the presence of maghemite particles has not disturbed the equation of state of laponite.

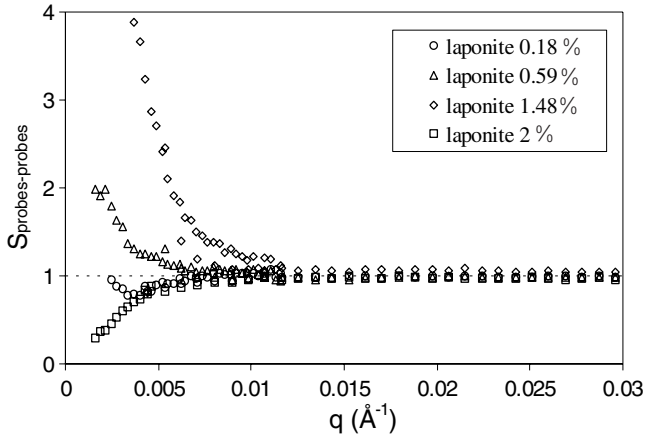

Figure 9. The effective structure factor of magnetic probes in hybrid systems. Φ_{probes} is constant (0.05%). Φ_{laponite} corresponds respectively to part 1 of the equation of state ($\Phi = 0.18\%$), the beginning ($\Phi = 0.59\%$) and end of part 2 ($\Phi = 1.48\%$) and part 3 ($\Phi = 2\%$) [14].

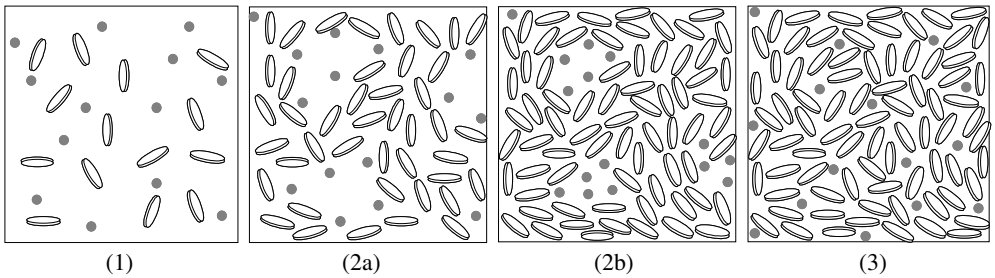

Figure 10. Schematic diagrams of the laponite suspensions including magnetic probes ($\Phi = 0.05\%$). The small spheres represent the maghemite nanoparticles and the discs the laponite clay platelets. Pictures (2a) and (2b) correspond respectively to the beginning and the end of the pseudoplateau where solid-like domains of clay coexist with liquid-like pockets. Pictures (1) and (3) depict the pure liquid phase and the pure solid phase (gel) respectively [14].

4. Ferrofluids and liposomes

'Magnetoliposomes' have been introduced by De Cuyper [39] to describe iron oxide nanoparticles wrapped in a lipid bilayer. Small and large magnetic liposomes have been studied in recent years as regards applications in the field of biotechnology [40], because of their compatibility with biological media combined with their physical properties. In particular, their ability to move in a magnetic field gradient (a phenomenon called magnetophoresis) is useful for sorting processes. With a much larger size (10 μm and above), giant magnetoliposomes exhibit important deformations when a magnetic field is applied (figure 11). From the analysis of such shape modifications, it has been possible to get some information on the membrane properties. For example, the membrane bending modulus of DOPC (1, 2-dioleoyl-sn-glycero-3-phosphocholine) has been estimated [11].

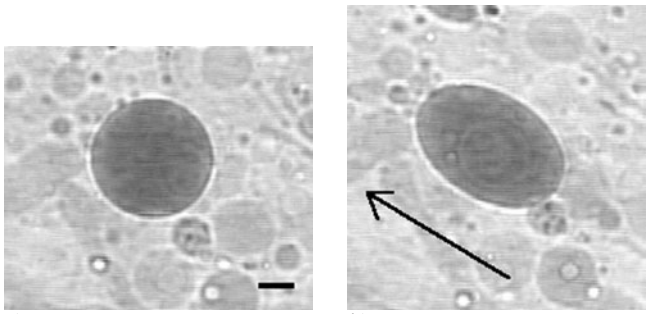

Figure 11. Magnetic field-induced deformation of giant magnetoliposomes. The length of the bar is 10 μm. The field intensity is $H = 0$ (a) and $H = 3 \times 10^{-3}$ T (b). The arrow shows the direction of the field.

4.1. CitMF: a good candidate for encapsulation

Several procedures are possible for encapsulating nanoparticles in liposomes but two conditions are always required. The particles have to be negatively charged, in order to avoid quick adsorption of the phospholipid molecules on their surface, and coated by citrate species, in order to be dispersed in water at pH 7. The residual tri-sodium citrate in solution is sometimes a problem for applications, but its concentration can be adjusted through dialysis of the magnetic fluid against a tri-sodium citrate solution of the desired concentration.

Here the total osmotic pressure of the encapsulated magnetic fluid (osmotic pressure due to the particles + osmotic pressure due to the ionic species) is a key factor for the synthesis of the magnetoliposomes as for their stability. The problem is not a problem of the phase diagram, because liposomes are out-of-equilibrium objects, but is related to the properties of the membrane and to the swelling of the liposomes. The ionic strength has to be especially carefully controlled because it will affect the properties of the final magnetoliposome.

4.2. Encapsulation of CitMF in giant liposomes

Particles can be introduced in the liposomes either by a multiple emulsion process [8], or by a spontaneous swelling in water of phospholipid bilayers filled with magnetic particles, or by the swelling of the phospholipidic bilayers in a magnetic fluid followed by the separation of the non-encapsulated particles [41]. The procedure is chosen according to the size required for the final liposomes.

Giant unilamellar magnetic liposomes have been obtained by spontaneous swelling in water of phospholipid bilayers pre-hydrated with an aqueous magnetic fluid. The phospholipid powder (1 mg) is mixed with 10 μl of CitMF and sheared on a glass support. Thus an oily orange film is obtained, which is then swollen with distilled water (1 ml) at 45 °C.

The first remark is that the swelling is more efficient when the film is pre-hydrated by a solution of charged particles and ions rather than pure water. Indeed, the water added in excess to the multi-lamellar film swells the system in order to dilute the material entrapped in the phospholipid bilayers (the charged magnetic particles and the unadsorbed tri-sodium citrate). The low diffusion coefficient of the particles enables their encapsulation while the swelling process of the lipid bilayers takes place, whereas the tri-sodium citrate electrolyte diffuses rapidly in the surrounding medium.

If water is added under flow and in a restricted volume (for example directly in the observation chamber, of 200 μm thickness), liposomes connected to tubes are observed

Figure 12. An optical picture of the preparation obtained by spontaneous swelling of a phospholipid bilayer stuffed with magnetic particles in water. The water is added under flow in the observation cell. The tube and liposome are linked together; the ferrofluid is inside the structure. The bar length is 20 μm.

(figure 12). Such phospholipidic tubes have already been described [42]. The novelty of the present system lies in the action of the magnetic fluid on the tube itself but also on the liposomes ending each tube. Pearling instability has thus been induced in such tubes by the stress of the two ending liposomes due to the application of a magnetic field [43].

The population of the liposomes obtained by spontaneous swelling is heterogeneous in size and in colour, indicating that the concentration of magnetic particles is not the same in all liposomes. Because of the swelling process, these two characteristics cannot be calculated using a simple dilution factor, but both the volume fraction of magnetic particles and the concentration of tri-sodium citrate inside liposomes can be determined at the end. Magnetophoresis experiments, i.e. migration in a controlled magnetic field gradient, allow an estimation of the volume fraction Φ of magnetic particles encapsulated inside the liposomes (ranging between 0.002 and 0.005%). The concentration of tri-sodium citrate encapsulated in the liposomes is obtained from the observation by optical microscopy of a liposome in a solution of known salinity. When the ionic strength is the same inside and outside the liposome, the latter appears as a sphere with a fluctuating membrane.

4.3. Deswelling of giant magnetoliposomes

Shape transitions are well-known consequences of osmotic stress on red blood cells or on liposomes [44]. An increase of the osmotic pressure outside liposomes induces a decrease of their diameter that is related to the flow of water toward the outside of the liposomes across the lipid membrane. The same kind of phenomenon was observed with magnetoliposomes, the osmotic stress being induced by an increase of the salt concentration outside the liposomes [45]. Quantitative characterization of the deswelling process was performed by direct measurement of the vesicle radius as a function of time for different values of the concentration gradient across the phospholipid membrane, Δc (figure 13(a)). The permeability of the DOPC bilayer to water measured for Δc ranging between 7 and 70 m mol l^{-1} has been found to be equal to 34 μm s^{-1}, in good agreement with the values found in other studies. It has to be underlined that

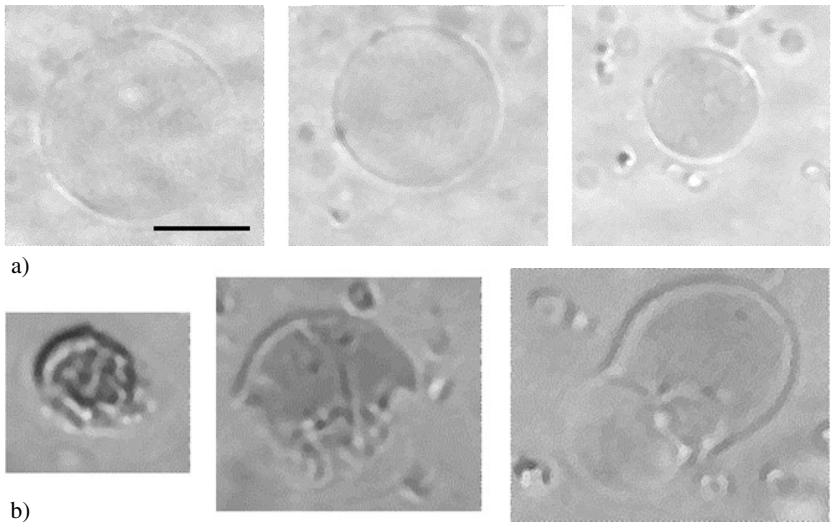

Figure 13. (a) Optical microscopy of a magnetoliposome subjected to a concentration gradient $\Delta c = 7$ m mol l^{-1}. The diameter of the liposome decreases due to a water flow toward the outer medium. The bar length is 10 μm. (b) Reswelling of a magnetoliposome that has been previously subjected to an osmotic stress.

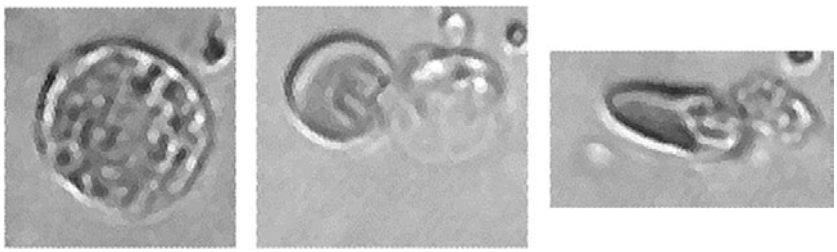

Figure 14. The last stage of the osmotic stress. The inner phase becomes more and more contrasted and exhibits a large deformation under a weak magnetic field ($H = 0.03$ T).

throughout the deswelling process, at the same time as the diameter of the liposomes decreases, the latter becomes more and more orange coloured, indicating an increase of its particle volume fraction. This indicates that the nanoparticles are unable to permeate the liposome surface, thereby suggesting the absence of mesoscopic pores during the osmotic stressing inducing the deswelling process. Magnetic nanoparticles appear here as possible probes for testing the formation of mesoscopic pores in a membrane. In most cases, the deswelling process leads to a drop of concentrated magnetic fluid being stuck to a phospholipid membrane without any apparent release of magnetic material in solution. This drop exhibits an important deformation when a magnetic field of 0.03 T is applied, attesting to the high concentration of magnetic material and the presence of an excess of phospholipid membrane (figure 14). On decreasing the osmotic pressure in the surrounding medium by water dilution, this object begins to swell again. At the end, a spherical liposome filled with the magnetic fluid is recovered, with almost the same size as before the osmotic stress was applied (figure 13(b)). The reswelling process appears here as proof that the membrane is not dramatically damaged during the deswelling process.

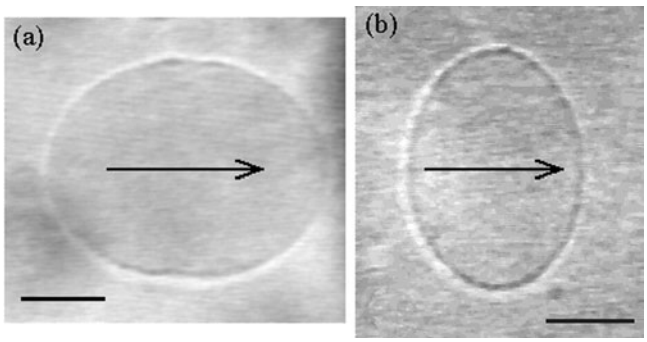

Figure 15. Optical pictures of the two kinds of shape exhibited by a magnetoliposome under the application of a magnetic field [47]: (a) a prolate ellipsoid for a high-ionic-strength ferrofluid; (b) an oblate ellipsoid for a low-ionic-strength ferrofluid. The length of the bar is 10 μm.

4.4. Deformation of giant magnetoliposomes

An illustration of the importance of the encapsulated ferrofluid composition is the effect of the ionic strength upon the magnetic field-induced deformations of liposomes. At high ionic strength, the application of a magnetic field of low intensity (0.04 T) to a giant magnetoliposome elongates the latter in the direction of the field (prolate ellipsoids; see figure 15(a)). Conversely, at low ionic strength, the same magnetic field compresses the liposomes at their poles (oblate ellipsoids; see figure 15(b)). The relevant experimental parameters for explaining this shape transition are the initial radius R_0 of the liposome, the magnetic susceptibility χ and the salt concentration C_s in the encapsulated ferrofluid. Two domains corresponding to both types of deformation are defined on a shape phase diagram, the oblate one being in the region of low values of R_0, χ and C_s [46]. A model comparing the magnetic energy and the bending energy of the membrane enabled the sensitivity of the shape to C_s to be established [47]. The main result of this description is an anisotropic distribution of particles in the neighbourhood of the membrane when a magnetic field is applied. This shape transition triggered by the ionic strength is explained by an electrostatic interaction between the weakly charged phospholipid bilayer and the ionic encapsulated species (particles and Na_3Cit electrolyte)

4.5. Conclusions

This last part illustrates that the inclusion of a citrate-stabilized ferrofluid (CitMF) in liposomes allows the probing of some properties of the latter and helps with the interpretation of their behaviour. Again the composition of the ferrofluid, especially the ionic strength, is a key parameter, as it controls the osmotic pressure of the systems. Giant liposomes are useful objects, as they allow a direct observation of the effect of a physical control such as the magnetic field, or a chemical modification of the system. For example, mesoscopic pores or complete solubilization of the phospholipid membrane can be observed on addition of a detergent to giant magnetoliposomes. Once again the magnetic nanoparticles appear as possible probes. At a lower scale, small magnetoliposomes (LUV, 200 nm in diameter) are now under study [41]. In this case, a direct observation is not possible and only averaged quantities can be determined. Nevertheless, they have applications in the field of pharmacology and it is interesting to draw a parallel between the behaviour of the magnetic giant and that of large vesicles.

5. General conclusions

This paper illustrates, through three examples, the versatility of CitMF for making magnetic composite materials in aqueous media. The main interest of the specific magnetic properties of nanoparticles for the composite material was in performing mechanical measurements on the other components of the system over a large range of scales: macroscopic (the stretching test for ferrogels and the possibility of magnetostriction), microscopic (the deformation of giant liposomes under a magnetic field) and nanoscopic (the local viscosity in laponite suspensions).

The key point is the robustness of CitMF, which remains stable whatever the conditions of ionic strength and magnetic field in the pH stability range of the nanoparticles. Perfect knowledge of the interaction strength and range through the osmotic pressure has allowed us to set conditions of osmotic pressure for several purposes:

- For making stable ferrogels and tuning their swelling and elastic properties through variation of the magnetic particle concentration.
- For using nanoparticles in an interaction range where they behave as non-invasive probes.
- For exploring the swelling and deswelling of liposomes in response to an osmotic stress.

One may wonder about the possibility of doping with magnetic nanoparticles some composite materials that are not stable within the same physicochemical range as CitMF. Other chemical conditions of colloidal stability of such particles can be found by coating their surfaces with ligands other than citrate, surfactants [48], silica [49], or simply by using 'naked' particles (bare iron oxide). Controlling the initial osmotic pressure of the precursor suspension of nanoparticles is still the prerequisite for ensuring the stability of the particles in the final product.

Acknowledgments

All these results were obtained thanks to a close collaboration with Delphine Talbot, Emmanuelle Dubois, Pierre Levitz, Régine Perzynski, Jean-Claude Bacri and Jean Chevalet. The part of this work concerning ferrogels was supported by CONACYT Mexico.

References

[1] Chaput F, Boilot J-P, Canva M, Brun A, Perzynski R and Zins D 1993 *J. Non-Cryst. Solids* **160** 177–79
[2] Haas W, Zrínyi M, Kilian H G and Heise B 1993 *Colloid Polym. Sci.* **271** 1024–34
[3] Mayer C, Cabuil V, Lalot T and Thouvenot R 2000 *Adv. Mater.* **12** 417
[4] Berejnov V, Raikher Yu, Cabuil V, Bacri J C and Perzynski R 1998 *J. Colloid Interface Sci.* **199** 215
[5] Fabre P, Casagrande C, Veyssié M, Cabuil V and Massart R 1990 *Phys. Rev. Lett.* **64** 53
[6] Bibette J 1993 *J. Magn. Magn. Mater.* **122** 37
[7] Fermigier M and Gast A P 1993 *J. Magn. Magn. Mater.* **122** 46
[8] Ménager C and Cabuil V 1995 *J. Colloid Interface Sci.* **169** 251
[9] Bacri J-C, Dumas J, Gorse D, Perzynski R and Salin D 1985 *J. Physique Lett.* **46** L1199
[10] Berejnov V, Bacri J-C, Cabuil V, Perzynski R and Raikher Yu 1998 *Europhys. Lett.* **41** 507
[11] Bacri J-C, Cabuil V, Cebers A, Ménager C and Perzynski R 1996 *Europhys. Lett.* **33** 235
[12] Ménager C, Belloni L, Cabuil V, Dubois M, Gulik-Krzywicki T and Zemb Th 1996 *Langmuir* **12** 3516
[13] Cousin F, Dubois E and Cabuil V 2002 submitted
Cousin F, Dubois E, Cabuil V, Boué F and Perzynski R 2001 *Braz. J. Phys.* **31** 350
[14] Cousin F, Cabuil V and Levitz P 2002 *Langmuir* **18** 1466–73
[15] Massart R 1981 *IEEE Trans. Magn.* **17** 1247
[16] Massart R, Dubois E, Cabuil V and Hasmonay E 1995 *J. Magn. Magn. Mater.* **149** 1
[17] Dubois E, Boué F, Cabuil V and Perzynski R 1999 *J. Chem. Phys.* **111** 7147
[18] Cousin F and Cabuil V 1999 *J. Mol. Liq.* **83** 203

[19] Dubois E, Perzynski R, Boué F and Cabuil V 2000 *Langmuir* **16** 5617–25
[20] Cousin F, Dubois E and Cabuil V 2001 *J. Chem. Phys.* **115** 6051–7
[21] Cousin F and Cabuil V 2000 *Prog. Colloid Polym. Sci.* **115** 77
[22] Xu X, Friedman G, Humfeld K D, Majetich S A and Asher S A 2002 *Chem. Mater.* **14** 1249–56
[23] Muniz E C and Geuskens G 2001 *Macromolecules* **34** 4480–4
[24] Benguigui L and Boué F 1999 *Eur. Phys. J.* B **11** 439–44
[25] Flory P J 1953 *Principles of Polymer Chemistry* (Ithaca, NY: Cornell University Press) pp 576–94
[26] Philipova O E, Rulkens R, Kovtunenko B I, Abramchuck S S, Khokhlov A R and Wegner G 1998 *Macromolecules* **31** 1168–79
[27] Takata S I, Norisuye T and Shibayama M 1999 *Macromolecules* **32** 3989–93
[28] Bajpai A K and Bajpai S K 1995 *Colloids Surf.* A 10121–28
[29] Nisato G, Munch J-P and Candau S J 1999 *Langmuir* **15** 4236–44
[30] Nikitin L V, Mironova L S, Stepanov G V and Samus A N 2001 *Vysokomol. Soedin.* A **43** 698–706 (Engl. transl. 2001 *Polym. Sci.* A **43** 443–50)
[31] Mitsumata T, Ikeda K, Gong J P, Osada Y, Szabó D and Zrínyi M 1999 *J. Appl. Phys.* **85** 8451–5
[32] Mourchid A, Delville A, Lambard J, Lécolier E and Levitz P 1995 *Langmuir* **11** 1942–50
[33] Kroon M, Wegdam H G and Sprik R 1996 *Phys. Rev.* E **54** 6541
[34] Pignon F, Piau J-M and Magnin A 1996 *Phys. Rev. Lett.* **56** 3281–9
[35] Bonn D, Kellay H, Tanaka H, Wegdam G and Meunier J 1999 *Langmuir* **15** 7534–6
[36] Levitz P, Lécolier E, Mourchid A, Delville A and Lyonnard S 2000 *Europhys. Lett.* **49** 672
[37] Mourchid A, Lécolier E, Van Damme H and Levitz P 1998 *Langmuir* **14** 4718–23
[38] Gabriel J C P, Sanchez C and Davidson P 1996 *J. Phys. Chem.* **100** 11139–43
[39] de Cuyper M and Joniau M 1988 *Eur. Biophys. J.* **15** 311
[40] Bulte J W M, De Cuyper M, Despres D and Frank J A 1999 *J. Magn. Reson. Imaging* **9** 329–35
[41] Lesieur S, Grabielle-Madelmont C, Ménager C, Cabuil V, Dahdi D, Pierrot P and Edwards K 2002 submitted
[42] Bar-Ziv R, Tlusty T, Moses E, Safran S A and Bershadsky A 1999 *Proc. Natl Acad. Sci. USA* **96** 10140
[43] Ménager C, Meyer M, Cabuil V, Cebers A, Bacri J-C and Perzynski R 2002 *Eur. Phys. J.* E **7** 325–37
[44] Boroske E, Elwenspoek M and Helfrich W 1981 *Biophys. J.* **34** 95
[45] Ménager C and Cabuil V 2002 *J. Phys. Chem.* B **106** 7913–18
[46] Sandre O, Ménager C, Prost J, Cabuil V, Bacri J-C and Cebers A 2000 *Giant Vesicles* ed P L Luisi and P Walde (Chichester: Wiley) pp 169–80
[47] Sandre O, Ménager C, Prost J, Cabuil V, Bacri J-C and Cebers A 2000 *Phys. Rev.* E **62** 3865–70
[48] Massart R, Roger J and Cabuil V 1995 *Braz. J. Phys.* **25** 135–41
[49] Cousin F, Cabuil V, Ménager C and Levitz P 2002 submitted